ELSEVIER

Contents lists available at ScienceDirect

# International Journal of Non-Linear Mechanics

journal homepage: www.elsevier.com/locate/nlm



# On the double resonance activation of electrostatically actuated microbeam based resonators



Hassen M. Ouakad <sup>a,\*</sup>, Mohammad H. Hasan <sup>b</sup>, Nizar R. Jaber <sup>c</sup>, Md Abdullah Al Hafiz <sup>d</sup>, Fadi Alsaleem <sup>b</sup>, Mohammad Younis <sup>c</sup>

- <sup>a</sup> Department of Mechanical and Industrial Engineering, Sultan Qaboos University, PO Box 33, Al-Khoudh, Muscat, Oman
- <sup>b</sup> Mechanical Engineering Department, University of Nebraska Lincoln, Lincoln, NE, USA
- <sup>c</sup> Physical Sciences and Engineering Division, King Abdullah University of Science and Technology, Thuwal, Kingdom of Saudi Arabia
- <sup>d</sup> School of Mathematics and Physics, The University of Queensland, St Lucia QLD 4072, Australia

#### ARTICLE INFO

# Keywords: MEMS Microbeam Sensor Actuator Double resonance Mechanical resonance Electrical resonance

#### ABSTRACT

Electrostatically actuated microelectromechanical system (MEMS) devices have shown prominent potential in various applications. However, despite their low power consumption, they do require high input voltages to be actuated. This is even worse if these devices are driven around their mechanical resonant state. Assuming a double resonance excitation scheme, both electrically and mechanically, activates the system's mechanical and electrical resonances simultaneously. This double resonance activation was recently verified experimentally to alleviate the problem of high actuating voltage/displacement near the resonant state. Therefore, in this work, an analytical electro-mechanical coupled model for a double-resonance-driven microbeam, assuming a classical nonlinear beam model combined with an RLC electric circuit model is first proposed and then numerically examined. Good match among the numerical simulations and the experimental data when the electrical resonance frequency band is sufficiently high is demonstrated. The suggested model can be used to further optimize certain MEMS designs and therefore fully benefit from this double resonance activation scheme in improving MEMS sensors and actuators.

#### 1. Introduction

Microelectromechanical systems (MEMS) have been utilized in a wide range of applications including: micro-resonators [1–4], micro-gyroscopes [5], resonant micro-sensors [6–12], micro-gyroscopes [13] and micro-switches [14], and more recent emerging applications such as logic gates and computing units [15–18]. Electrostatic MEMS are among the most popular types of MEMS devices because of their attractive properties such as their ease of fabrication, rapid response time, and low power requirements. Nevertheless, because of the weakness of electrostatic forcing, even at the microscopic scale, MEMS devices require large input voltages to actuate them. This requirement limits the use cases of MEMS devices and curb their potential [19].

A large body of research exists to explore different means of amplifying the response of MEMS devices using mechanical resonance activation and design parameter optimization [20,21]. The parameter optimization includes increasing the surface area to intensify the actuating electrostatic force effect or reducing the MEMS structure stiffness to reduce stiffness force. However, the new optimized parameters may result in negative consequences such as intensifying the squeezefilm damping (SQFD) effect [22] and accordingly the possibility of

introducing dynamical instabilities such as pull-in and stiction (short circuit) [23]. Parametric resonance was also proposed to increase the response of MEMS devices and enhance their output signal [24-26]. Yet, utilizing parametric resonance requires a challenging actuation mechanism or compound structures to modulate the MEMS stiffness. Moreover, it requires strict low damping conditions to reduce activation voltage [27] and increase the width of the parametric resonance instability tongues [28,29]. Aside from mechanical amplification approaches, electrical resonance was previously used under the term "resonance drive" to amplify the electrical signal fed into the MEMS device statically [30-37]. The concept was later employed in a dynamic fashion to create a MEMS demodulator [37] by feeding the MEMS device with amplitude-modulated or frequency-modulated signals [37] to improve the response of the MEMS device while avoiding actuating it close to its resonant frequency not to hit the dynanic pull-in instability. Finally, recently, our group has introduced the concept of double resonance excitation by simultaneously activating the MEMS resonator's primary mechanical and electrical resonances [30,31] through a simple, mixed frequency excitation signal [32-34]. Much like [37] this activation is passive and results in high voltage gains compared to the typical mechanical resonance activation.

E-mail address: houakad@squ.edu.om (H.M. Ouakad).

Corresponding author.

It is noted that, despite the progress that has been achieved into theoretically and experimentally improving MEMS devices output signals through several activation schemes, all of these require complex actuation mechanisms/structures, that are not easy to implement, and involve complicated optimization patterns. Therefore, it would be of great advantage to MEMS designers to be able to use simple model as well as design for enhancing MEMS devices stokes without the need to hit any mechanical resonant instability and at the same time, further increase their output signals. Consequently, in this work, a theoretical investigation of the concept of double resonance excitation in a MEMS resonator is carried out. A new nonlinear coupled electro-mechanical model for the coupled system to complement the experimental data is

The organization of this paper is as follows: in Section 2, a mathematical model of the mechanical and electrical components of the MEMS device is first proposed. A double resonance excitation is introduced in Section 3. The experimental setup to characterize the MEMS device and its respective circuitry is summarized in Section 4. Numerical discretization process of the model equations is outlined in Section 5. In Section 6, the simulation results and experimental data to validate the model equations are summarized; The potential use of electrical resonance for static amplification in MEMS devices is then suggested in Section 7. Finally, results discussion and appropriate conclusions are established in Section 8.

#### 2. Mathematical formulation

#### 2.1. Mechanical model

The examined MEMS device consists of a composite doubly-clamped microbeam, as shown in Fig. 1(a). The beam is composed of layers of chrome (Cr), gold (Au), and polyimide. The material and geometrical properties of each layer are shown in Fig. 1 and also summarized in both Tables 1 and 2. The cross-sectional view of beam is shown in Fig. 1(b). When unforced, the MEMS flexible upper is separated from the stationary bottom electrode by a gap of width  $d = 3.3 \mu m$ . The beam dynamics are governed by the following classical Euler-Bernoulli nonlinear beam equation [29,38]:

$$(EI)_{eff} \frac{\partial^{4} w}{\partial x^{4}} + (\rho A)_{eff} \frac{\partial^{2} w}{\partial t^{2}} + c \frac{\partial w}{\partial t}$$

$$= \frac{(EA)_{eff}}{2L} \left( \int_{0}^{L} \left( \frac{\partial w}{\partial x} \right)^{2} \right) \frac{\partial^{2} w}{\partial x^{2}} + F_{electrical} \left( w \left( x, t \right) \right), \tag{1}$$

with the following respective doubly-clamped boundary conditions [29]:

$$w(x = 0, t) = w(x = L, t) = 0; \frac{\partial w}{\partial x}(x = 0, t) = \frac{\partial w}{\partial x}(x = L, t) = 0$$
 (2)

where w(x, t) is the deflection of the beam about its unforced equilibrium position as a function of the position x and time t. It is worth noting that microbeam deflection is denoted as positive when the upper electrode deflects towards bottom electrode (downward motion) and negative when it deflects away. In the same equation,  $(EI)_{eff}$ symbolizes the effective product of the Young's modulus and moment of inertia of the composite microbeam,  $(\rho A)_{eff}$  represents the product of the effective mass density and cross-sectional area, c represents the viscous damping coefficient, L is the microbeam length, b is its width, h is its thickness, and  $F_{electrical}$  is the electrostatic forcing acting on the microbeam per unit length. It is worth mentioning that the effective single-layer beam model parameters ((EI)<sub>eff</sub>, ( $\rho A$ )<sub>eff</sub>, and (EA)<sub>eff</sub>) were all extracted for the actual multi-layer beam using the method of transformed sections, as explained in the paper Appendix.

The selected microbeam in this work consisting of a composite microbeam, Fig. 1b, is fabricated on a silicon wafer coated with 500 nm of thermally grown silicon dioxide (SiO2) layer. The lower actuating electrode were formed by patterning the Cr/Au layer that is sputtered on the wafer surface and having an overlapping width with the upper

Composite microbeam layers geometrical and material properties.

Layer material	Thickness (nm)	Young modulus (Gpa)	Mass density (kg/m³)
Chrome (Cr)	50	279	7190
Gold (Au)	200	79	19300
Polyimide (Pm)	4300	8.5	1400

Composite microbeam equivalent geometrical dimensions

1 0	
Composite length (L)	400 μm
Overlapping width (b)	10 μm
Composite total thickness (h)	4.85 μm
Initial gap size (d)	3.3 µm

composite microbeam of  $b = 10 \mu m$ . The composite upper microbeam itself was made of a 4.2 µm polyimide layer coated from top with 50/200 nm Cr/Au layer. This layer is used to define the beam dimensions and act as hard mask to protect the beam during the reactive ion etching (RIE). The upper electrode is formed by coating the beam from bottom with 50/200/50 nm of Cr/Au/Cr layers, respectively. The Cr layer is used to enhance the adhesion of the polyimide layer with other materials. The two electrodes are separated by 3.3 µm amorphous silicon layer. This layer is etched at the final stage of the fabrication to define the air gap.

When the MEMS circuit is assumed to be composed of only a voltage source and a MEMS capacitance, the voltage across the MEMS device is equal to the input voltage. In such case, the electrostatic force per unit length can be written as follows:

$$F_{electrical}\left(w\left(x,t\right)\right) = \frac{\varepsilon b V_{in}^{2}}{2\left(d-w\left(x,t\right)\right)^{2}}\tag{3}$$

Alternatively, Eq. (3) can be expressed as a function of the accumulated charge across the MEMS capacitance as follows:

$$F_{electrical}\left(w\left(x,t\right)\right) = \frac{\varepsilon bQ^{2}\left(t\right)}{2\left[C_{tot}\left(d-w\left(x,t\right)\right)\right]^{2}}\tag{4}$$

where Q(t) is the charge accumulated in the system's equivalent capacitance,  $C_{tot}$ . It is worth observing that Eq. (3) and Eq. (4) are equivalent. However, Eq. (4) is more convenient to analyze electrical resonance, as will be further explained in the sub-sequent section.

# 2.2. Electrical model

The MEMS device electrical component can be modeled as a variable capacitance  $C_{MEMS}$ . This capacitance is assumed to be in parallel to a parasitic capacitance,  $C_n$  (Fig. 2), that arises from the imperfections in the circuit and the properties of external connections such as BNC cables. The total (equivalent) circuit capacitance is given by Eq. (5) and Eq. (6):

$$C_{tot}(x,t) = C_p + C_{MEMS}(x,t)$$
(5)

$$C_{tot}(x,t) = C_p + C_{MEMS}(x,t)$$

$$C_{MEMS}(x,t) = \frac{\varepsilon bL}{(d-w(x,t))}$$
(6)

Electrical resonance requires an LC circuit. Therefore, an external inductor,  $L_e$ , is added (not to be confused by the microbeam length, L). Introducing  $L_e$  inevitably introduces a small parasitic resistance,  $R_e$ .  $L_e$  and  $R_e$  are modeled as passive elements in series with the circuit equivalent capacitance, as shown in Fig. 2. Thus creating a series resonating RLC (resistor-inductor-capacitor) circuit with an electrical resonance frequency  $f_{electrical}$  given by (7):

$$f_{electrical}(x,t) = \frac{1}{2\pi} \frac{1}{\sqrt{LC_{-}(x,t)}}$$
 (7)

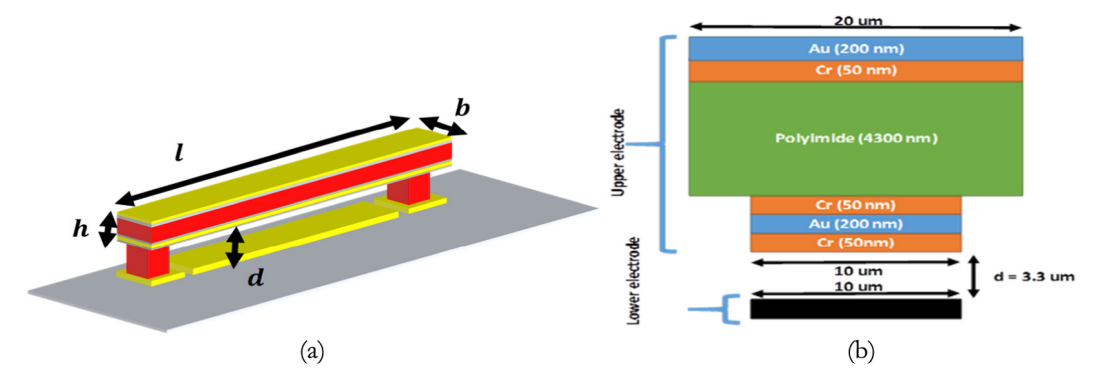


Fig. 1. (a) 3D schematic of the clamped-clamped microbeam. (b) Cross-sectional view of the composite microbeam (not to scale).

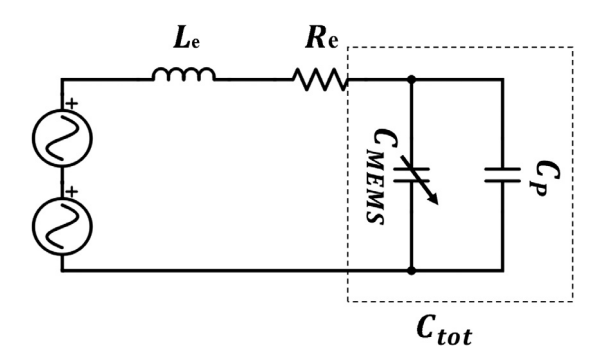


Fig. 2. A simplified model of the MEMS equivalent circuit.

The RLC series circuit response can be expressed by the following second order differential equation:

$$L_{e} \frac{d^{2}Q(t)}{dt^{2}} + R_{e} \frac{dQ(t)}{dt} + \frac{1}{C_{tot}(x,t)} Q(t) = \sum V_{in}(t)$$
 (8)

where  $\sum V_{in}(t) = \sum_i V_{AC_i} \cos\left(2\pi f_i t\right)$  is the summation of the input actuating voltage signals. As the electrical system is governed by a second-order differential equation, if the system is sufficiently underdamped, it exhibits a large response around its electrical resonance frequency. This leads to a large build-up charge across the capacitances in the circuit, and it corresponds to a voltage amplification across the MEMS device. Considering the cases where the electrical resonance is significantly far from the mechanical resonance, the following uncoupled, simplified, model can be alternatively used [31]:

$$E'I\frac{\partial^{4}w}{\partial x^{4}} + (\rho A)_{eff}\frac{\partial^{2}w}{\partial t^{2}} + c\frac{\partial w}{\partial t} = \frac{(EA)_{eff}}{2L} \left(\int_{0}^{L} \left(\frac{\partial w}{\partial x}\right)^{2}\right) \frac{\partial^{2}w}{\partial x^{2}}$$

$$+ \frac{\varepsilon b \left(\sum_{in} \frac{V_{in}(t)}{\sqrt{\left(\tilde{\Omega}_{in}R_{e}(C_{tot})\right)^{2} + \left(1 - \tilde{\Omega}_{in}^{2}L_{e}(C_{tot})\right)^{2}}}\right)^{2}}{2(d-w)^{2}}, \tag{9}$$

where  $\tilde{\Omega}_{in} = \tilde{\Omega}_1, \tilde{\Omega}_2, \ldots, \tilde{\Omega}_n$  represents the frequency of the input signals actuating the MEMS device. Eq. (9) assumes that the microbeam vibrates quasi-statically compared to the faster electrical response of the RLC circuit.

#### 3. Double resonance excitation

If the MEMS primary mechanical resonance and its circuit electrical resonance frequencies are equal, a double resonance can be simply activated by exciting the MEMS circuit using a single AC signal around the resonance frequency of the MEMS device. More generally, in the case of frequency disparity, a multi-frequency AC signal [33,34] can be used to activate the double resonance as follows:

$$V_{in}(t) = V_{AC1}\cos(2\pi f_1 t) + V_{AC2}\cos(2\pi f_2 t)$$
 (10)

where  $V_{ACi}$  and  $f_i$  are the voltage amplitude and frequency of the  $i^{\rm th}$  AC harmonic source, respectively. The coupled micro mechanical and electrical system responds to the above assumed two frequency components  $f_1$  and  $f_2$  (superposition principle) while the mechanical system reacts to the following frequency components due to the quadratic forcing term in Eq. (3):

$$0(DC), 2f_1, 2f_2, (f_1 - f_2), (f_1 + f_2),$$
 (11)

Thus, it is possible to trigger two distinct resonance in the system by choosing appropriate combinations of input frequency components. The simultaneous activation of mechanical and electrical resonances was previoully explored and discussed in detail in [31].

#### 4. Experimental setup

The MEMS device introduced in Section 2 was mechanically and electrically characterized using the experimental setup in Fig. 3. The deflection of the MEMS device was captured using a laser Doppler vibrometer while the voltage across the MEMS capacitance was monitored using a digital multimeter. The MEMS device was driven by an input voltage using a national instruments DAQ module.

The MEMS primary mechanical resonance frequency was revealed to be around 116 kHz by performing a frequency sweep of the MEMS device using a one AC and one DC source at atmospheric pressure (Fig. 4a). The response is achieved with  $V_{DC} = 30 \text{ V}$  and a variety of AC voltages. Electrical characterization is influenced by the microbeam deflection as its capacitance is a function of the separation width. Therefore, the electrical response is attained by actuating the microbeam at low voltage to maintain the MEMS capacitance nearly constant. The electrical resonance frequency can be tuned by changing the inductance of the MEMS circuit via a variable inductor. The electrical gain of the circuit can also be tuned by changing the resistance of the circuit. It is noted here that increasing the inductance of the circuit will inevitably result in a larger circuit resistance due to the introduction of a larger parasitic resistance. The electrical resonance frequency of the RLC circuit is found at the frequency corresponding the maximum voltage across the MEMS device (Fig. 4b) or the maximum conductance (minimum impedance) of the circuit (Fig. 4c).

Fig. 4c illustrates the electrical circuit response at two inductor values: when  $L_e=4$  mH,  $f_{electrical}=116$  kHz  $\cong f_{mechanical}$ , and when  $L_e=0.5$  mH,  $f_{electrical}=304$  kHz, which represents a typical frequency mismatch case. It can be observed here that the circuit quality factor, Fig. 4c, predictably decreases as the inductance increases due to the increase in the parasitic resistance of the circuit as depicted in the following equation:

$$Q_e = \frac{1}{R_e} \sqrt{\frac{L_e}{C_{tot}}} \tag{12}$$

where  $Q_e$  represents the electrical quality factor.

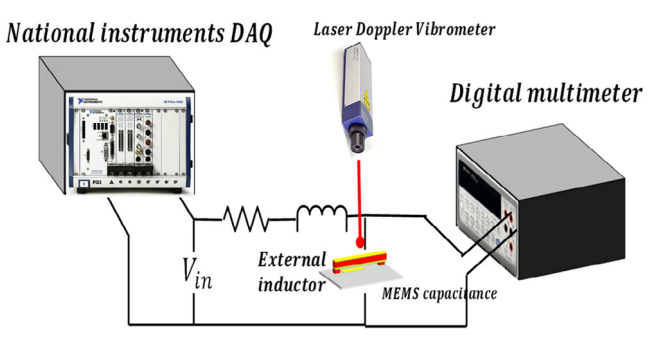


Fig. 3. Experimental setup for mechanical and electrical characterizations.

#### 5. Galerkin based modal expansion

In this work, the Galerkin modal decomposition was used to solve the MEMS dynamic equations. To this end, the Galerkin expansion technique was used to get an approximate numerical solution w(x,t) for the coupled equations governing the MEMS-based resonator dynamics as follows [29]:

$$w(x,t) = \sum_{i=1}^{n} \psi_i(x) \,\mu_i(t),$$
(13)

where  $\psi_{i=1..n}(x)$  are the basis functions (i.e. the linear undamped mode-shapes of a clamped–clamped beam). The functions  $\mu_i(t)$  denote time-varying generalized coordinate functions. To acquire the reduced order model (ROM) of the coupled problem, Eqs. (13) was substituted into Eqs. (8) and (9) and the outcome equation was then multiplied by the trial modeshape functions  $\psi_{j=1..n}(x)$ . The resultant ROM equations

were then integrated in time using Runge–Kutta technique. It is also worth saying here that as the modeshapes remain embedded inside the denominators of the electrostatic force term in the ROM. Thus, the spatial integrals containing the modeshapes are to be numerically evaluated while simultaneously integrating the differential equations of the modal coordinates. In this study, the first 5 modeshapes (i = 5) of the ROM were shown to be sufficient to capture the system dynamics. Validation of the assumed 5-modes ROM convergence study can be found in [39–42].

To solve the nonlinear structural static behavior of the microbeam, the time-dependent terms in the ODEs were set to zero resulting in a system of nonlinear algebraic equations. The system was then solved numerically using the Newton–Raphson method.

#### 6. Model validation and experimental data

#### 6.1. Mixed frequency excitation case

The case of frequency mismatch by using an external inductance of 0.5 mH is first considered, which resulted in  $f_e=308$  kHz. The microbeam was driven at atmospheric pressure using a multi-frequency signal composed of two frequency components:  $f_1=f_{electrical}=308$  kHz with an amplitude  $V_{AC1}=6.5$  V. The other frequency component was swept between 170 kHz and 210 kHz such that  $f_1-f_2$  is near  $f_{mechanical}$ . The experimental data is presented in Fig. 5a along with simulation results of simultaneously solving (1) and (8) using the modal expansion technique. The figure shows good agreement between simulated experimental results. The fitting was obtained by setting the circuit parasitic resistance and the parasitic capacitance to  $R_e=120~\Omega$  and  $C_p=469$  pF, respectively. This extracted parasitic capacitance is quite high. It is understood here that the parasitic capacitance is due

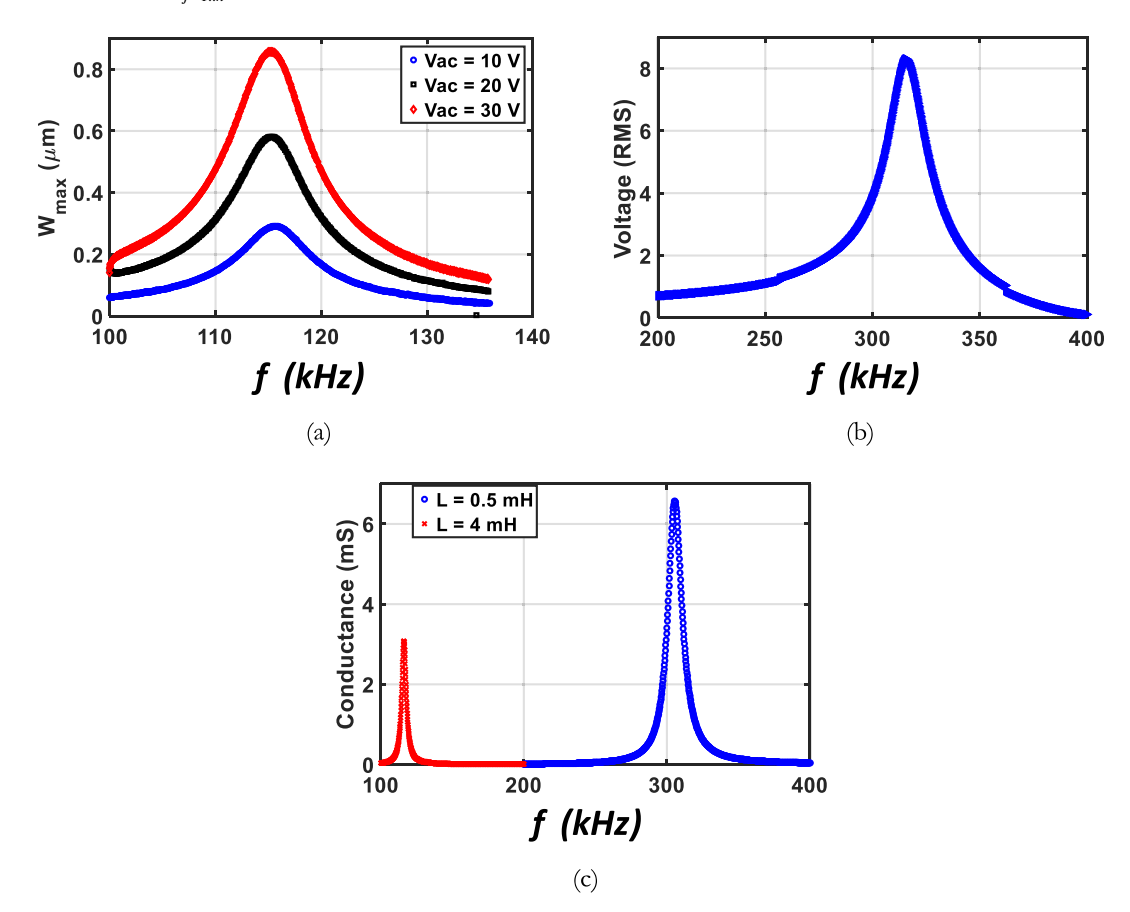


Fig. 4. Experimental electromechanical system characterization performed at atmospheric pressure. a: Mechanical characterization using  $V_{DC} = 30$  V and various AC voltages. b: Electrical characterization through voltage monitoring using  $L_e = 0.5$  mH and  $V_{AC} = 282.8$  mV RMS. c: Electrical characterization through various electrical conductance values.

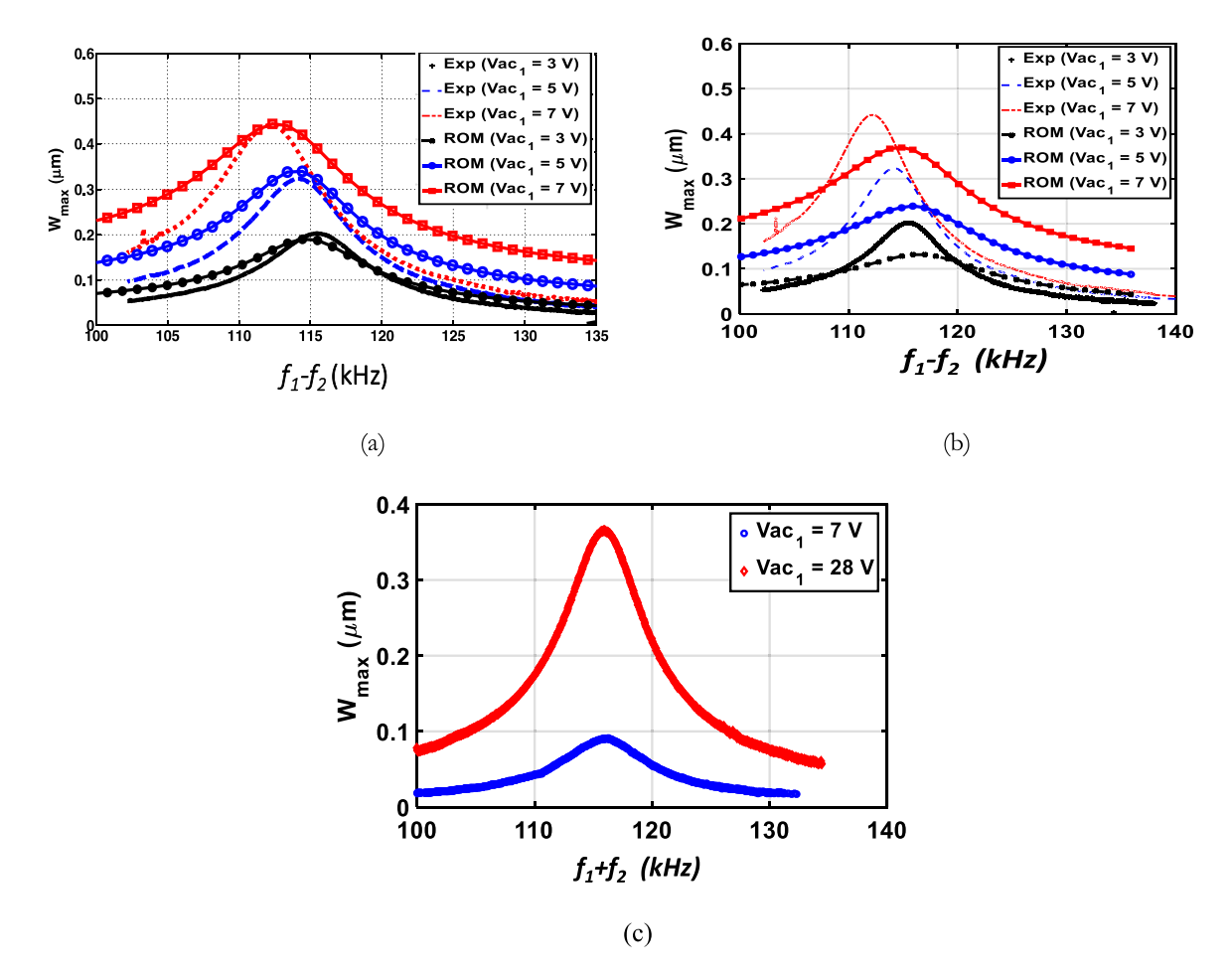


Fig. 5. (a) Multi-frequency response obtained experimentally at atmospheric pressure.  $f_1 = 308$  kHz,  $V_{AC2} = 6.5$  V,  $f_2 = [170$  kHz-210 kHz] while  $V_{AC1}$  is varied. The experimental data are shown as unmarked lines and the simulation results are shown as marked lines with the same colors as the experimental one. (b) Another comparison between experimental and simulation results using the simplified electrical response in (9). (c) Multi-frequency excitation without activating electrical resonance:  $f_1 = 80$  kHz,  $V_{AC2} = 42$  V and  $f_2 = [20$  kHz-60 kHz]. The assumed amplitudes of  $V_{AC1}$  are shown in the figure legend.

to using biaxial cables to connect the MEMS device to the power supply and the network analyzer. These cables introduce quite a large parasitic capacitance to the system. Moreover, because of the operation being implemented at relatively high frequencies, it is believed that some parasitic capacitance components may have become noticeable within the assumed circuit itself (such as a capacitance between the bonded wires and a parasitic capacitance between the MEMS sensing electrode, moving electrode and actuating electrode). It is noted here that the circuit parasitic parameters were fitted assuming a simple linear RLC model that might not necessarily capture the actual representation in the system. This approach allows to model a complex, continuous electrical model using simple and lumped elements.

Next, the experimental data were compared to the simulation results obtained by the approximative model of Eq. (9). Fig. 5b shows that using Eq. (9) results in a higher deviation between the experimental results and the numerical simulations.

Double resonance activation results in large voltage amplification, which facilitates the high MEMS deflection shown in Fig. 5a. To further elucidate on this argument, Fig. 5c shows the response of the composite MEMs microbeam to a multi-frequency excitation signal with  $f_1+f_2$  but with no individual component equal to the electrical resonance frequency. In this case, one needs to introduce significantly higher input voltage ( $V_{AC1}=28~\rm V$ ,  $V_{AC2}=42~\rm V$ ) to attain the same deflection as the double-resonance-driven MEMS ( $V_{AC1}=7~\rm V$ ,  $V_{AC2}=6.5~\rm V$ ).

#### 6.2. Simple double resonance case

If the mechanical and electrical resonance frequencies are comparable (i.e.  $f_{mechanical} \cong f_{electrical}$ ), it is possible to activate double resonance without the need for a multi-frequency excitation signal. In this case, a common DC signal superimposed with an AC signal can be used. Frequency matching was achieved by setting  $L_e = 4$ mH. It is worth asserting here that a DC signal is needed in order to avoid frequency doubling bifurcation in the mechanical response, thus ensuring the MEMS device resonates at a frequency equal to the input signal frequency. Fig. 6 compares experimental data with simulation results for the frequency response of the matched-frequency microbeam. In this case, unlike the frequency mismatch case in Fig. 5a, the simulation results are less accurate. This discrepancy is likely to be due to the simplified circuit used in this work, as the electrical circuit is simply assumed to be a series RLC circuit. In reality, the actual circuit is very likely to be more complex than that. If the MEMS device vibrates at a frequency far from the electrical resonance frequency, the series RLC circuit assumption holds well, as shown in Fig. 5(a). However, when the micro-system is driven around the electrical resonance, with  $f_{mechanical} = f_{electrical}$ , the circuit inaccuracy becomes more pronounce as the MEMS device oscillates within the timescale of the circuit. We plan to address this point by proposing a more accurate circuit model in a future work.

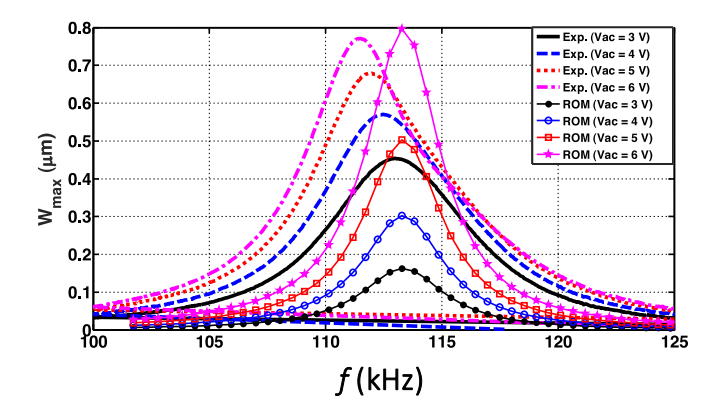


Fig. 6. The frequency response of the system using  $L_e=4$  mH,  $R_e=118~\Omega,~V_{DC}=10$  V and varying AC voltages. The experimental results are shown in unmarked lines and the simulation results are shown in marked lines.

#### 7. Electrical resonance as a static response amplifier

After validating the model, another possible advantage of electrical resonance actuation, even in case of a frequency mismatch, is the ability to amplify the static deflection of MEMS devices, as previously demonstrated by [35,36]. This is because of the quadratic relationship between the input voltage forcing and the electrostatic forcing. Thus, the electrostatic actuation force using a single AC signal with a frequency  $f_a >> f_m$  can be approximated as:

$$F_e(w(x,t))$$

$$= \frac{\varepsilon b}{2(d-w)^2} \frac{\left[0.5V_{in}^2 + 0.5V_{act}^2 Cos\left(4\pi f_e t\right)\right]}{\left[\left(\left(2\pi f_e\right)R_e C_{tot}\left(x,t\right)\right)^2 + \left(1 - \left(2\pi f_e\right)^2 L_e C_{tot}\left(x,t\right)\right)^2\right]}$$
(14)

As the MEMS device attenuates signals with frequencies that far exceed its resonance frequency, the term  $0.5V_{in}^2Cos\left(4\pi f_e t\right)$  in the numerator is negligible. Thus, the forcing in (14) is static with an amplified amplitude. It is worth noting here that the gain attained using this approach is not constant as the total capacitance of the system depends on the MEMS deflection. The gain is highly variable when  $C_{tot}$ "- $\cong C_{MEMS}$  since the MEMS deflection will shift the electrical resonance frequency of the system away from the supply signal frequency, which is typically constant. This shift would reduce the gain of the system. This interaction can be seen as an internal feedback in the system. Interestingly, increasing the parasitic capacitance of the MEMS system tends to eliminate this internal feedback effect if the parasitic capacitance far exceeds the MEMS variable capacitance. In this case, the capacitance change due to the MEMS deflection will have a negligible effect on the overall capacitance of the system, which leads to a nearly constant electrical resonance frequency during operation.

Fig. 7 theoretically demonstrates the effects of parasitic capacitance on the response of the electrical resonance-driven MEMS device using the following input signal parameters  $f_1=116$  kHz,  $f_{electrical}=308$  kHz and  $V_{DC2}=V_{AC2}=0$  Volt. The voltage  $V_{AC1}$  was swept to show the effects of internal negative feedback at higher deflection for different ratios between the paratactic capacitance and the MEMS nominal capacitance  $C_p/C_{MEMS}$  values. As anticipated, increasing this ratio reduces the internal negative feedback and increases the deflection of the MEMS device.

#### 8. Results discussion and conclusion

The response of a MEMS device under double resonance activation was simulated using the Galerkin modal expansion for coupled and uncoupled mechanical–electrical models. A key challenge that was to be

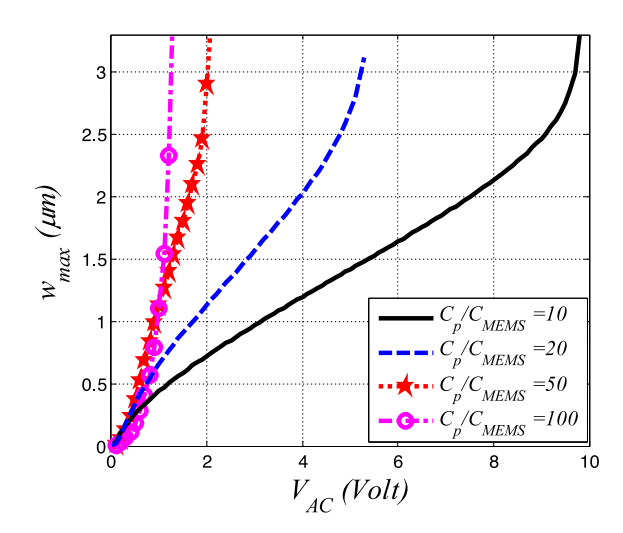


Fig. 7. The use of electrical resonance as a means to enhance the static response of MEMS devices by increasing the MEMS deflection due to voltage amplification. The voltage amplification is more pronounced when  $C_{\rm p}/C_{\rm MEMS}$  is high.

confronted in this work is that the basis functions of the Galerkin modal expansion remain embedded in the denominators of the nonlinear electrostatic force term. This was handled by simultaneously evaluating the spatial integrals containing the basis functions numerically while integrating the motion differential equations of the MEMS device. The simulation results for both models were compared with experimental data. In this comparison, the coupled model showed a better fit with the experimental data, especially when the MEMS device has a mechanical natural frequency that is different from the MEMS electrical circuit natural frequency (a frequency mismatch).

As most MEMS systems are expected to operate with a frequency mismatch, the findings in this work suggest that the coupled model may be sufficient for capturing the behavior of double resonance in most MEMS applications. However, there is still a room to improve the coupled model by utilizing a more comprehensive electromagnetic model and by accounting for the fringing fields effects in the MEMS circuit model. These model improvements are planned as the subject of a future study.

In conclusion, in this work, a theoretical and experimental investigation of electrical resonance activation in a composite MEMS microbeam was carried out. The mechanical subsystem was modeled using the Euler–Bernoulli beam equation while the electrical subsystem was modeled using a simple RLC. Coupling between the MEMS subsystems occurs via the electrostatic forcing term. As each subsystem is second order in nature, both subsystems can achieve a large input amplification at their perspective resonance frequencies. When both resonances are activated simultaneous (double resonance activation), the response of the MEMS device is significantly amplified. This double resonance activation was shown to provide high voltage amplification and an enhanced response both dynamically and statically.

## **Declaration of competing interest**

The authors declare that they have no known competing financial interests or personal relationships that could have appeared to influence the work reported in this paper.

### Appendix. Equivalent beam model

To simplify the study of our composite microbeam, an equivalent beam model to represent our microbeam as a single layer beam using the equivalent area method is utilized. The neutral axis of the singlelayer equivalent beam was attained by considering a beam with the

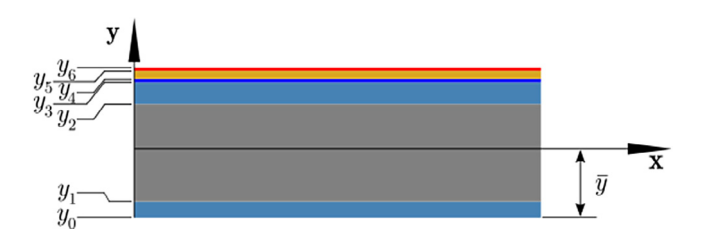


Fig. A.1. Neutral axis of the multi-layered microbeam.

same first moment of area as that of the composite beam. Thus, the position of the single-layer microbeam,  $\bar{y}$ , is obtained using (a1):

$$\bar{y}\sum_{i=1}^{6} A_i = \sum_{i=1}^{6} A_i y_i \tag{A.1}$$

where  $y_i$  represents the location of the neutral axis of layer i along the y-axis, and  $A_i$  is the cross-sectional area of layer i calculated by adjusting the width of every layer such that  $b_{i,eff} = b_i E_i / E1$  (see Fig. A.1).

After calculating the neutral axis position, it is possible to find the effective modulus of elasticity of the single-layer microbeam,  $I_{eff}$  using the parallel axis theorem on the microbeam transformed section:

$$I_{eff} = \sum_{i=1}^{6} I_i \tag{A.2}$$

where  $I_i$  is the second moment of inertia of layer i that can be computed as follows:

$$I_1 = \frac{b_1 h_1^3}{12} + b_1 h_1 \left(\frac{h_1}{2} - \overline{y}\right)^2 \tag{A.3}$$

$$I_{i} = \frac{b_{i}h_{i}^{3}}{12} + b_{i}h_{i} \sum_{j=1,j< i} \left(h_{j} + \frac{h_{i}}{2} - \overline{y}\right)^{2}$$
(A.4)

where  $h_i$  and  $b_i$  are the thickness and width of layer i, respectively, shown in Fig. 1 and Table 1. Finally, the effective flexural rigidity,  $(EI)_{eff}$ , and mass per unit length,  $(\rho A)_{eff}$  can be attained by simply summing the flexural rigidity and mass per unit length of all layer in the composite microbeam:

$$\begin{cases} (EI)_{eff} = \sum_{i=1}^{6} E_{i}I_{i} \\ (\rho A)_{eff} = \sum_{i=1}^{6} \rho_{i}A_{i} \end{cases}$$
(A.5)

#### References

- [1] V. Kumar, J.W. Boley, Y. Yang, H. Ekowaluyo, J.K. Miller, G.T.C. Chiu, J.F. Rhoads, Bifurcation-based mass sensing using piezoelectrically-actuated microcantilevers, Appl. Phys. Lett. 98 (15) (2011) 153510.
- [2] H. Li, B. Balachandran, Buckling and free oscillations of composite microresonators, J. Microelectromech. Syst. 15 (1) (2006) 42–51.
- [3] H. Li, B. Piekarski, D.L. DeVoe, B. Balachandran, Nonlinear oscillations of piezoelectric microresonators with curved cross-sections, Sensors Actuators A 144 (1) (2008) 194–200.
- [4] M. Tausiff, H.M. Ouakad, H. Alqahtani, A. Alofi, Local nonlinear dynamics of MEMS arches actuated by fringing-field electrostatic actuation, Nonlinear Dynam. 95 (4) (2019) 2907–2921.
- [5] H.M. Ouakad, Nonlinear structural behavior of a size-dependent MEMS gyroscope assuming a non-trivial shaped proof mass, Microsyst. Technol. 26 (2020) 573-582
- [6] Y. Kessler, S. Krylov, A. Liberzon, Flow sensing by buckling monitoring of electrothermally actuated double-clamped micro beams, Appl. Phys. Lett. 109 (8) (2016) 083503
- [7] X.M.H. Huang, M. Manolidis, S.C. Jun, J. Hone, Nanomechanical hydrogen sensing, Appl. Phys. Lett. 86 (14) (2005) 143104.
- [8] B. Ilic, Y. Yang, K. Aubin, R. Reichenbach, S. Krylov, H.G. Craighead, Enumeration of DNA molecules bound to a nanomechanical oscillator, Nano Lett. 5 (5) (2005) 925–929.

- [9] D.R. Southworth, L.M. Bellan, Y. Linzon, H.G. Craighead, J.M. Parpia, Stress-based vapor sensing using resonant microbridges, Appl. Phys. Lett. 96 (16) (2010) 163503.
- [10] M.H. Hasan, H.M. Ouakad, F. Alsaleem, On the effects of temperature and relative humidity on the response of a MEMS arch resonator, in: ASME 2017 International Design Engineering Technical Conferences and Computers and Information in Engineering Conference, American Society of Mechanical Engineers Digital Collection, 2017.
- [11] M.H. Hasan, F.M. Alsaleem, H.M. Ouakad, Novel threshold pressure sensors based on nonlinear dynamics of MEMS resonators, J. Micromech. Microeng. 28 (6) (2018) 065007.
- [12] N. Kacem, S. Baguet, S. Hentz, R. Dufour, Computational and quasi-analytical models for non-linear vibrations of resonant MEMS and NEMS sensors, Int. J. Non-Linear Mech. 46 (3) (2011) 532–542.
- [13] A. Frangi, G. Gobat, Reduced order modelling of the non-linear stiffness in MEMS resonators, Int. J. Non-Linear Mech. 116 (2019) 211–218.
- [14] D. Kalafut, A. Bajaj, A. Raman, Tristable capacitive microcantilever switches: Measurements and simulations, Int. J. Non-Linear Mech. 119 (2020) 103304.
- [15] A. Yao, T. Hikihara, Logic-memory device of a mechanical resonator, Appl. Phys. Lett. 105 (2014).
- [16] H. Nathanson, W. Newell, R. Wickstrom, J. Davis, The resonant gate transistor, IEEE Trans. Electron Devices 14 (3) (1967).
- [17] I. Mahboob, E. Flurin, K. Nishiguchi, A. Fujiwara, H. Yamaguchi, Interconnect-free parallel logic circuits in a single mechanical resonator, Nature Commun. 2 (2011).
- [18] A. Yao, T. Hikihara, Reprogrammable logic-memory device of a mechanical resonator, Int. J. Non-Linear Mech. 94 (2017) 406–416.
- [19] W.A. de Groot, J.R. Webster, D. Felnhofer, E.P. Gusev, Review of device and reliability physics of dielectrics in electrostatically driven MEMS devices, IEEE Trans. Device Mater. Reliab. 9 (2) (2009) 190–202.
- [20] H. Conrad, H. Schenk, B. Kaiser, S. Langa, M. Gaudet, K. Schimmanz, et al., A small-gap electrostatic micro-actuator for large deflections, Nature Commun. 6 (10078) (2015).
- [21] J.M. Huang, K.M. Liew, C.H. Wong, S. Rajendran, M.J. Tan, A.Q. Liu, Mechanical design and optimization of capacitive micromachined switch, Sensors Actuators A 93 (3) (2001) 273–285.
- [22] H. Hosaka, K. Itao, S. Kuroda, Damping characteristics of beam-shaped micro-oscillators, Sensors Actuators A 49 (1–2) (1995) 87–95.
- [23] W.M. Van Spengen, R. Puers, I. De Wolf, A physical model to predict stiction in MEMS, J, Micromech. Microeng. 12 (5) (2002) 702.
- [24] A. Eichler, J. Chaste, J. Moser, A. Bachtold, Parametric amplification and self-oscillation in a nanotube mechanical resonator, Nano Lett. 11 (7) (2011) 2699–2703.
- [25] R.B. Karabalin, X.L. Feng, M.L. Roukes, Parametric nanomechanical amplification at very high frequency, Nano Lett. 9 (9) (2009) 3116–3123.
- [26] I. Mahboob, H. Yamaguchi, Piezoelectrically pumped parametric amplification and q enhancement in an electromechanical oscillator, Appl. Phys. Lett. 92 (17) (2008) 173109.
- [27] W. Zhang, K.L. Turner, Application of parametric resonance amplification in a single-crystal silicon micro-oscillator based mass sensor, Sensors Actuators A 122 (1) (2005) 23–30.
- [28] K.L. Turner, S.A. Miller, P.G. Hartwell, N.C. MacDonald, S.H. Strogatz, S.G. Adams, Five parametric resonances in a microelectromechanical system, Nature 396 (6707) (1998) 149.
- [29] M.I. Younis, MEMS Linear and Nonlinear Statics and Dynamics, Springer, Berlin, 2011.
- [30] F.M. Alsaleem, M.H. Hasan, A novel low voltage electrostatic MEMS resonator sensor based on double resonance dynamic amplification, in: ASME 2017 Dynamic Systems and Control Conference, American Society of Mechanical Engineers, October 2017, p. V002T18A004.
- [31] M.H. Hasan, F.M. Alsaleem, N. Jaber, M.A.A. Hafiz, M.I. Younis, Simultaneous electrical and mechanical resonance drive for large signal amplification of micro resonators, AIP Adv. 8 (1) (2018) 015312.
- [32] N. Jaber, A. Ramini, M.I. Younis, Multifrequency excitation of a clampedclamped microbeam: Analytical and experimental investigation, Microsyst. Nanoeng. 2 (16002) (2016).
- [33] A. Ramini, A.I. Ibrahim, M.I. Younis, Mixed frequency excitation of an electrostatically actuated resonator, Microsyst. Technol. 22 (8) (2016) 1967–1974.
- [34] N. Jaber, A. Ramini, Q. Hennawi, M.I. Younis, Wideband MEMS resonator using multifrequency excitation, Sensors Actuators A 242 (2016) 140–145.
- [35] H.M. Ouakad, S. Ilyas, M.I. Younis, Investigating mode localization at lowerand higher-order modes in mechanically coupled MEMS resonators, J. Comput. Nonlinear Dyn. 15 (3) (2020).
- [36] M. Zamanzadeh, H.M. Ouakad, S. Azizi, Theoretical and experimental investigations of the primary and parametric resonances in repulsive force based MEMS actuators, Sensors Actuators A (2019) 111635.

- [37] S. Park, M. Pallapa, J. Yeow, E.M. Abdel-Rahman, Low voltage electrostatic actuation and angular displacement measurement of micromirror coupled with resonant drive circuit, IEEE IECON, Montreal, Canada, October 2012, pp. 3976–3981.
- [38] S.-R. Chung, S.Park, E.M. Abdel-Rahman, J.T.W. Yeow, M. Khater, Architecture for MEMS- based analog demodulation, J. Micromech. Microeng. 23 (2013) 045013
- [39] T.J. Anderson, A.H. Nayfeh, B. Balachandran, Coupling between high-frequency modes and a low-frequency mode: Theory and experiment, Nonlinear Dynam. 11 (1) (1996) 17–36.
- [40] S. Krylov, B.R. Ilic, D. Schreiber, S. Seretensky, H. Craighead, The pull-in behavior of electrostatically actuated bistable microstructures, J. Micromech. Microeng. 18 (5) (2008) 055026.
- [41] K. Das, R.C. Batra, Symmetry breaking, snap-through and pull-in instabilities under dynamic loading of microelectromechanical shallow arches, Smart Mater. Struct. 18 (11) (2009) 115008.
- [42] H.M. Ouakad, F. Najar, Nonlinear dynamics of MEMS arches assuming out-of-plane actuation arrangement, J. Vib. Acoust. 141 (4) (2019) 041010.